Supporting Information

Sulfur-deficient MoS_2 grown inside hollow mesoporous carbon as a functional polysulfide mediator

Hong-En Wang,[*,a] Xuecheng Li,[a] Ning Qin,[c] Xu Zhao,[d] Hua Cheng,[c] Guozhong Cao[*,e] and Wenjun Zhang[*,b]

[a] State Key Laboratory of Advanced Technology for Materials Synthesis and Processing, Wuhan University of Technology, Wuhan 430070, China. Email: hongenwang@whut.edu.cn

[b] Center of Super Diamond & Advanced Films (COSDAF) and Department of Materials Science and Engineering, City University of Hong Kong, HKSAR, China. Email: apwjzh@cityu.edu.hk

[c] Department of Materials Science and Technology, Southern University of Science and Technology, Shenzhen 518055, China.

[d] Institute of Chemical Materials, China Academy of Engineering Physics, Mianyang 621900, China.

[e] Department of Materials Science and Engineering, University of Washington, Seattle, WA 98195, USA. Email: gzcao@u.washington.edu

Experimental section.

Synthesis of hollow mesoporous carbon (HMC) spheres.

The HMC was prepared by a simple one-pot self-assembly method referring literature.[1] Firstly, 3.46 mL of tetrapropyl orthosilicate (TPOS) solution was added into a mixed solution containing 70 mL of ethanol, 10 mL of deionized water and 3 mL of $NH_3 \cdot H_2O$ (25wt%) under vigorous stirring at room temperature. After 12 min, 0.4 g of resorcinol and 0.56 mL of formaldehyde (37wt%) were added to the above solution and the resultant mixture was vigorously stirring for 24 h. The resultant precursor was harvested by centrifugation, washed with deionized water and ethanol, and dried at 60 °C overnight. Then, the precursor was carbonized at 700 °C under Ar atmosphere for 5 h to obtain C/SiO_2 composite spheres. Finally, the HMC was obtained by removing the SiO_2 template using 4 M NaOH solution.

Synthesis of MoS_2/HMC and MoS_{2-x}/HMC composites.

The MoS_2/HMC was synthesized by a simple hydrothermal method without extra annealing. Typically, $NaMoO_4 \cdot 2H_2O$ (0.5 g) and thiourea ($CS(NH_2)_2$, 1.0 g) were dissolved into deionized water (30 mL) to form a transparent solution under vigorously stirring. Then, 100 mg HMC was added into the above solution under sonication for 1 h. Next, the resultant black mixture was transferred to a 60 mL Teflon-lined autoclave

and heated in an oven at 200 °C for 24 h. After that, the autoclave was naturally cooled to room temperature and the black precipitation was collected by centrifugation, washed several times with deionized water and ethanol, and finally dried at 60 °C in air. The MoS_{2-x}/HMC sample was obtained by annealing the MoS_2/HMC product at 800 °C for 2 h an in tube furnace under H_2/Ar (10% H_2) atmosphere.

Fabrication of HMC-S, MoS_2/HMC-S and MoS_{2-x}/HMC-S composite cathodes.

The HMC-S, MoS_2/HMC-S and MoS_{2-x}/HMC-S cathodes were all prepared by a conventional melt-diffusion method. In a typical procedure, the host material (HMC, MoS_2/HMC or MoS_{2-x}/HMC) and sulfur powders were uniformly mixed with a weight ratio 2:3, followed by heating at 160 °C for 20 h in a sealed vessel filled with Ar protection.

Structural characterization.

X-ray diffraction (XRD) patterns were recorded on a Bruker diffractometer with Cu Kα radiation (λ = 0.154056 nm). The morphology of the samples was observed by a Hitachi S-4800 scanning electron microscope (SEM). Transmission electron microscopy (TEM) and high-resolution transmission electron microscopy (HRTEM) micrographs were acquired on a JEOL JEM-2100F microscope. Scanning transmission electron microscopy (STEM) images and corresponding energy-dispersive X-ray

(EDX) mapping were obtained on JEOL JEM-2800 microscope. The specific surface area and pore size distribution were determined using Brunner–Emmett–Teller (BET) and Barrett–Joyner–Halenda (BJH) methods through N_2 adsorption/desorption isotherms at 77 K on a Tri Star II 3020 surface area and porosity analyzer. Prior to sorption experiments, the samples were degassed at 80 °C for 24 h under vacuum. The surface elemental composition and electronic states were analyzed by an X-ray photoelectron spectroscope (XPS, Thermo fisher, Alpha). The binding energies (BE) for the samples were calibrated using C 1s peak from a carbon tape at 284.8 eV. Thermogravimetry analyses (TGA) were recorded on a SETARAM Labsys Evo S60/58458 thermal analyzer under a flow of air (or Ar) with a heating rate of 5 °C min^{-1}. Raman measurements were recorded on a Renishaw inVia Raman Spectrometer with an excitation wavelength of 532 nm. Electron paramagnetic resonance (EPR) signals were measured using a Bruker EMX plus-10/12 with a Microwave Bridge (microwave frequency, 9.853 GHz; microwave power, 20 mW; modulation amplitude, 4 G; modulation frequency, 100 kHz) at room temperature.

Polysulfide adsorption experiments.

The Li_2S_6 solution (10 mM) were prepared by mixing sulfur and Li_2S with a stoichiometric molar ratio of 5:1 dissolved in DOL/DME (1:1, v/v) in an argon-filled glovebox. The resulting mixture was continuously stirred at 50 °C for 24 h to form a 10 mM Li_2S_6 stock solution. Then, 30 mg active material (HMC, MoS_2/HMC or MoS_2-

$_x$/HMC) was separately added into 3 mL of the above Li_2S_6 solution for static adsorption test.

Electrochemical measurements.

The electrochemical tests were performed using CR2025 coin cells with lithium foils as the counter/reference electrode and microporous membrane (Celgard 2400) as the separator. To make the working electrode, the active material (HMC-S, MoS_2/HMC-S or MoS_{2-x}/HMC-S), acetylene black, and polyvinylidene fluoride (PVDF) binder with a mass ratio of 8:1:1 in N-methyl-2-pyrrolidone (NMP) were fully blended to form a slurry. The slurry was uniformly coated on an Al foil and dried at 55 ^oC for 12 h under vacuum and then cut into circular disks with an average loading of 1.2 mg cm^{-2}. The electrolyte was 1.0 M solution of lithium bis(trifluoromethanesulfonyl)imide (LiTFSI) with 1wt% $LiNO_3$ dissolved in 1,3-dioxolane (DOL) and 1,2-dimethoxy ethane (DME) (1:1, v/v). The Li-S cells were assembled in an ultrapure argon-filled glovebox with both moisture and oxygen contents both below 0.3 ppm. Galvanostatic discharge–charge cycling was conducted using a LAND-CT2001A electrochemical workstation within a potential window of 1.4~2.8 V (vs. Li^+/Li) at different current densities. The cyclic voltammetry (CV) curves were measured at 0.2 mV s^{-1} on a CHI 604e electrochemical workstation. Electrochemical impedance spectroscopy (EIS) was recorded on an electrochemical workstation (Autolab PGSTAT 302N) at the frequency from 100 KHz to 0.01 Hz.

Symmetrical cell assembling and measurements.

The electrodes for symmetrical cells were assembled according to the literature method.[2] Firstly, 0.2 M Li_2S_6 solution was prepared by dissolving sulfur powder and Li_2S with a molar ratio of 5:1 in DOL/DME (1:1, v/v) without 1wt% $LiNO_3$ as electrolyte. Then, the active material (MoS_2/HMC or MoS_{2-x}/HMC) and PVDF binder with a mass ratio of 4:1 were dispersed in NMP to form a uniform slurry. The slurry was spread on aluminum foils and dried at 120 ^oC for 12 h under vacuum and then cut into circular disks as both working and counter electrodes. CV measurements of the symmetrical cells were tested at 2 mV s^{-1}.

Computational details.

All theoretical calculations were performed using DFT, as implemented in CASTEP code[3,4] from Materials Studio. The electron exchange and correlation energy was calculated using OTFG-type ultrasoft pseudopotential and Perdew–Burke–Ernzerhof (PBE) functional within the generalized gradient approximation (GGA). The electron–ion interactions were described within a plane–wave basis set with an energy cutoff of 500 eV. The *k*-point sampling was obtained from the Monkhorst-Pack scheme with a (2×2×1) mesh. The convergence criteria for SCF iteration and force were set to $1.0\times e^{-6}$ eV/atom and 0.03eV/Å, respectively. The 2H-MoS_2 surface slab was modeled

with a monolayer 3×3 supercell consisting of 27 atoms separated by a vacuum layer of 20 Å along the direction normal to the surface to avoid strong interactions between two adjacent layers. To model the $V_s^{\bullet\bullet}$, one S atom was removed from the MoS_2 surface slab.

The adsorption energies (E_{ads}) were calculated according to the following equation:

$$E_{ads} = E_{(\text{adsorbate/substrate})} - [E_{(\text{substrate})} + E_{(\text{adsorbate})}]$$

where $E_{(\text{adsorbate/substrate})}$, $E_{(\text{substrate})}$, and $E_{(\text{adsorbate})}$ represent the total energy of MoS_2 substrate with adsorbed polysulfide species, the clean MoS_2 substrate, and the polysulfide molecule in the gas phase, respectively. For adsorption energy calculations, the van der Waals interactions were considered using DFT-D method. The Li diffusion on the MoS_2 surface was simulated using LST/QST method.

Fig. S1 (a) SEM and (b) TEM images of the as-prepared hollow mesoporous carbon with abundant surface defects; (c, d) SEM of MoS_{2-x}/HMC product.

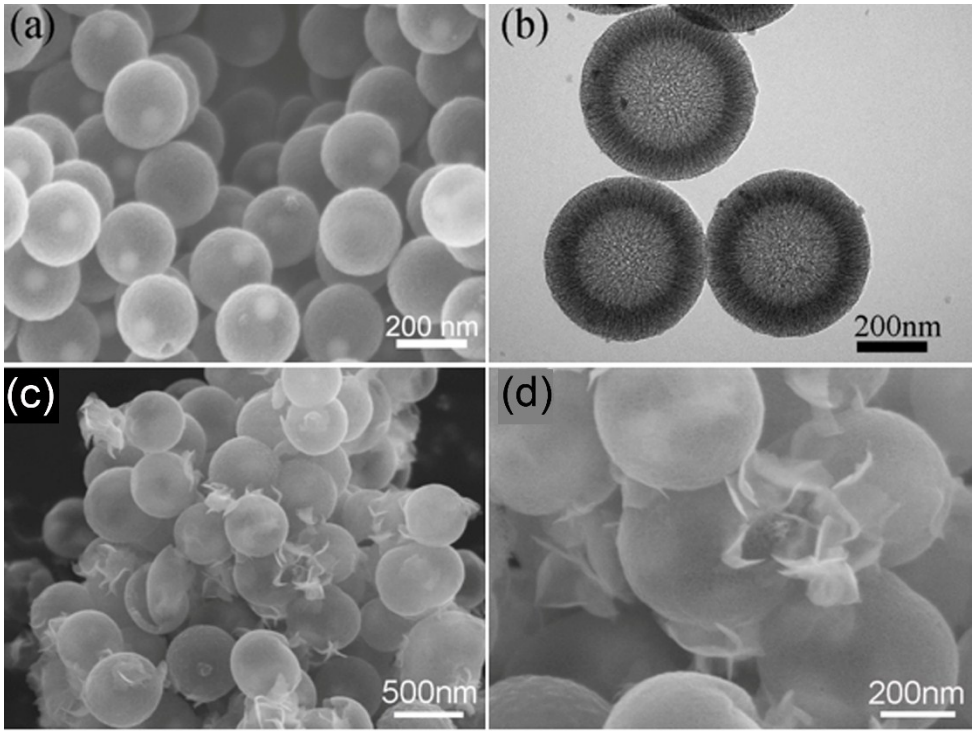

Fig. S2 (a) HRTEM, (b) an intensity line scan of region 1 marked by rectangle in (a), (c) IFFT image from (002) spot derived from FFT of region 2 in (a) using a filter, indicating the presence of a large number of edge sites.

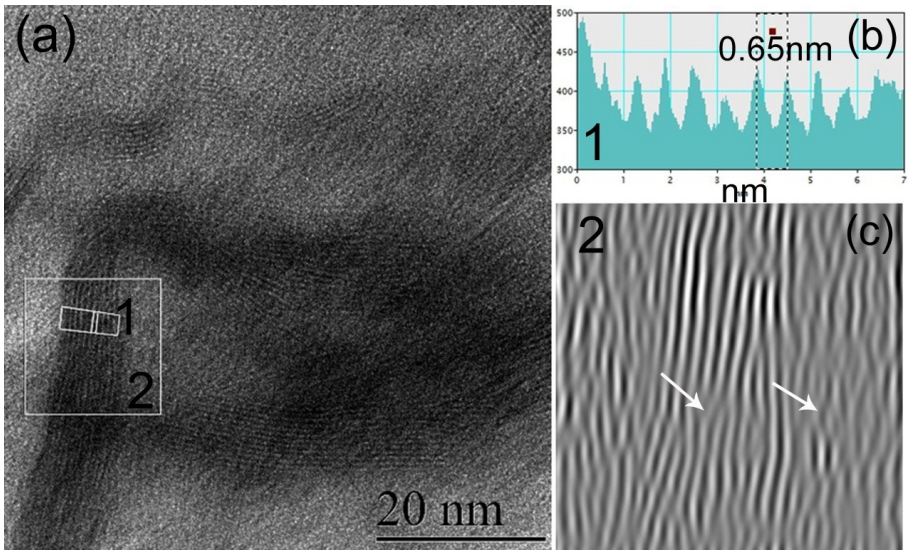

Fig. S3 N_2 sorption isotherms and pore size distribution plots (inset) of HMC (a), MoS_2/HMC and MoS_{2-x}/HMC samples (b).

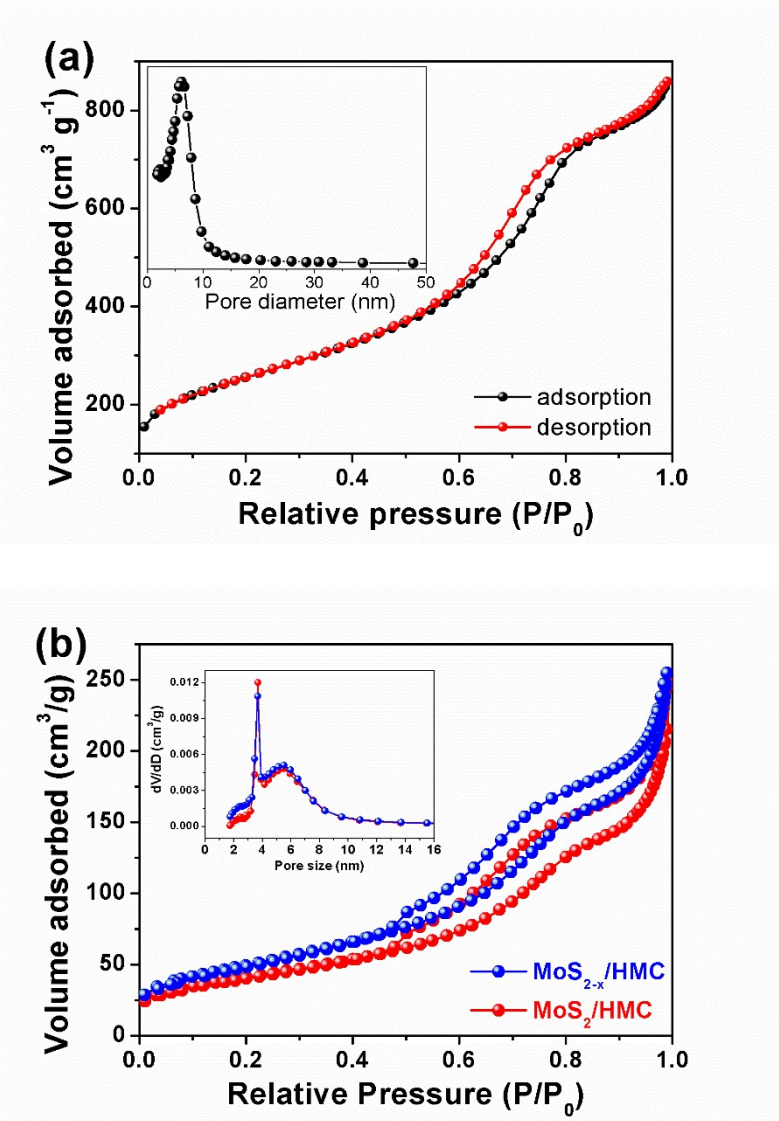

From Fig. S3a, the HMC product owns a high specific surface area of 892.1 m^2 g^{-1}) and pore volume of 1.31 cm^3 g^{-1} as summarized in Table S1. After deposition of MoS_2 nanosheets inside HMC, the resultant composite possesses a reduced specific surface area (146.6 m^2 g^{-1}) and pore volume (0.39 cm^3 g^{-1}) as shown in Fig. S3b.

Fig. S4 TGA/DSC curves of MoS_{2-x}/HMC sample in air.

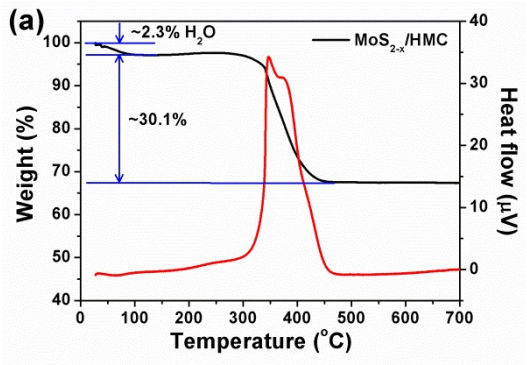

The weight fraction of MoS_2 in the MoS_{2-x}/HMC sample was determined by thermogravimetric (TG) and DSC analyses, as shown in Fig. S4. Upon combustion in air, the MoS_2 will be oxidized into MoO_3 and the underlying carbon spheres will be completely removed. Therefore, the mass contents of carbon and MoS_2 in the composite can be roughly estimated as 22.5% and 75.2%, respectively.

Fig. S5 (a) Raman spectra of the MoS_{2-x}/HMC and MoS_2/HMC samples, (b) C 1s XPS spectrum in MoS_{2-x}/HMC sample.

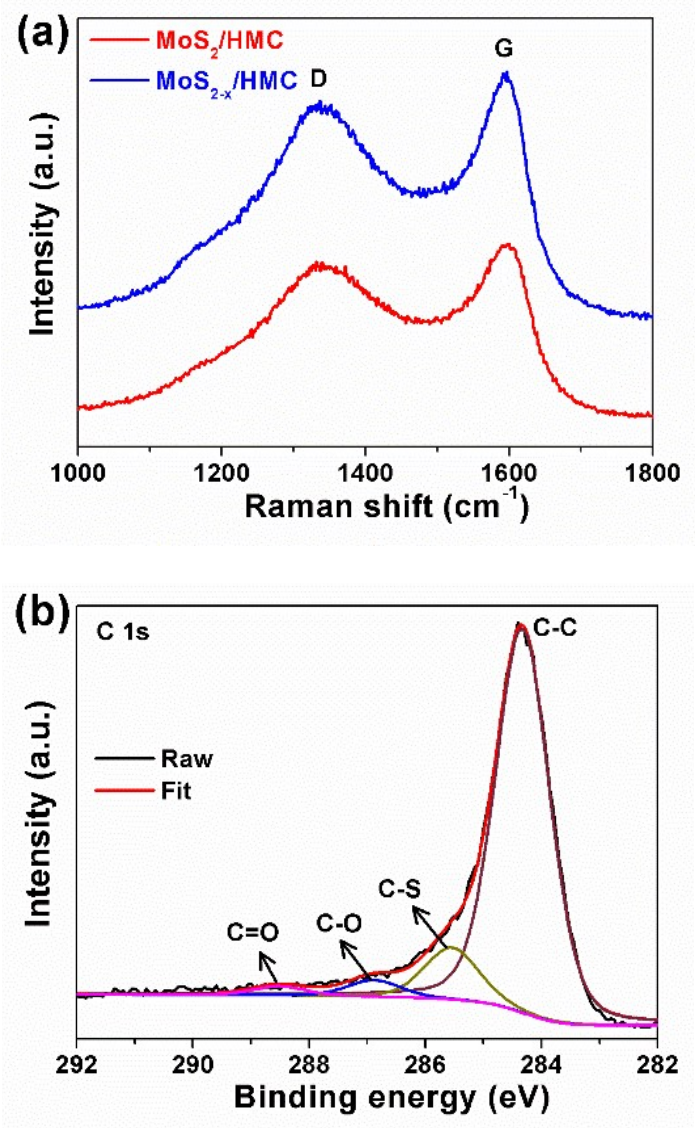

Fig. S6 Optimized geometrical configurations of Li_2S_4 adsorption (a, b) and Li diffusion (c, d) on pristine MoS_2 basal plane. (a, c) top and (b, d) tilted view. The cyan, yellow and pink balls represent Mo, S and Li atoms, respectively.

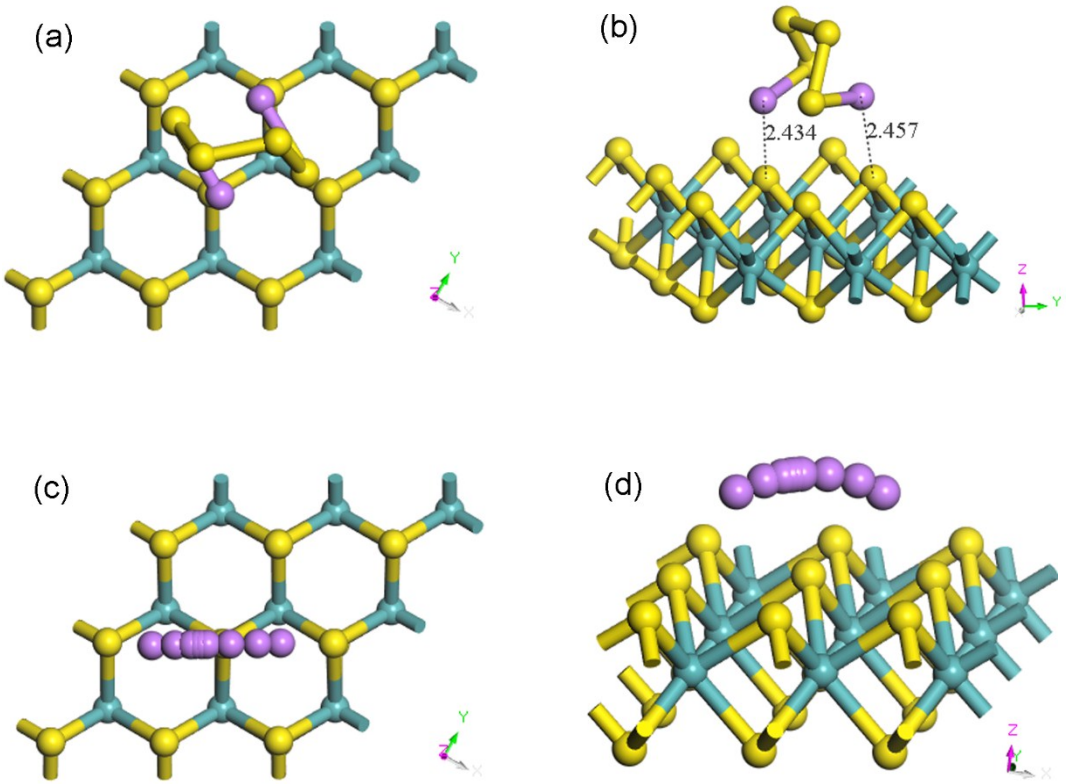

Fig. S7 (a) TGA curves of 3 samples loading with S and pure S in Ar (b) XRD patterns of MoS_{2-x}/HMC-S and MoS_2/HMC-S samples.

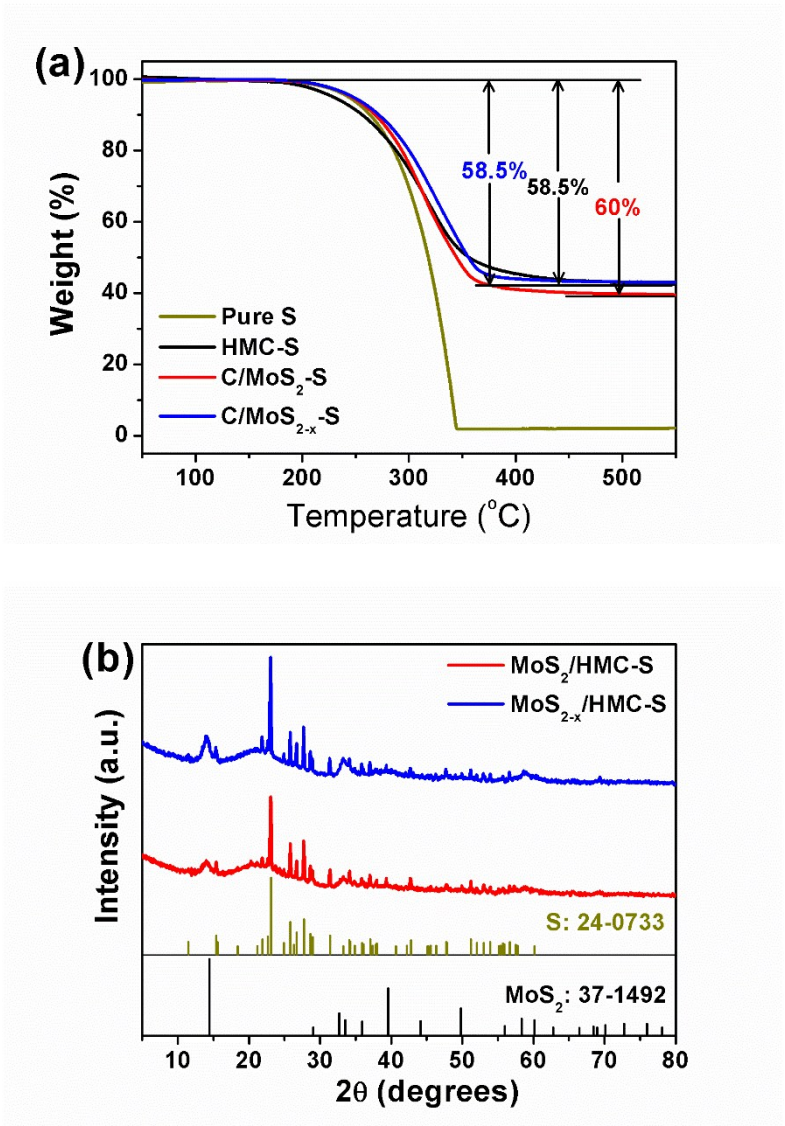

From TGA measurements (Fig. S7a), the weight fractions of S in the three composite cathodes were determined to be 58.5%, 58.5% and 60% for the MoS_{2-x}/HMC-S, HMC-S and MoS_2/HMC-S, respectively. In Fig. S7b, all the observed strong peaks (except those from the MoS_2 substrates) can be readily indexed to the monoclinic S (space group *Fddd*, JCPDS card no. 24-0733).

Fig. S8 SEM images of (a, d) HMC-S, (b, e) MoS_2/HMC-S and (c, f) MoS_{2-x}/HMC-S samples, suggesting that the sulfur species have been fully loaded inside the inner voids of the 3 hosts.

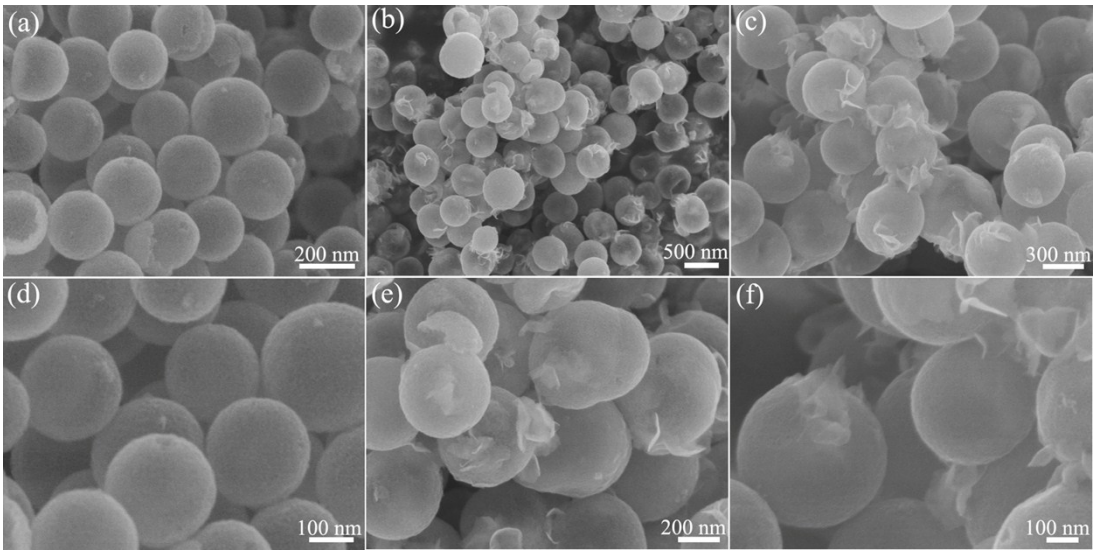

SEM images (Fig. S8) reveals the spherical morphologies of the carbon spheres covered by nanosheets have been well preserved after sulfur loading and no discrete sulfur clusters are observed, suggesting that most of sulfur has been filled inside the inner voids of the hollow carbon spheres.

Fig. S9 Electrochemical property of the MoS_{2-x}/HMC-S cathode. The first three cycles of (a) CV (0.2 mV s^{-1}) and (b) GCD curves, (c) selected GCD curves at 0.2 C, (d) GCD curves at different current rates, (e) long-term cycling performance at 3 C (the electrochemical property of MoS_2/HMC-S has been presented for comparison).

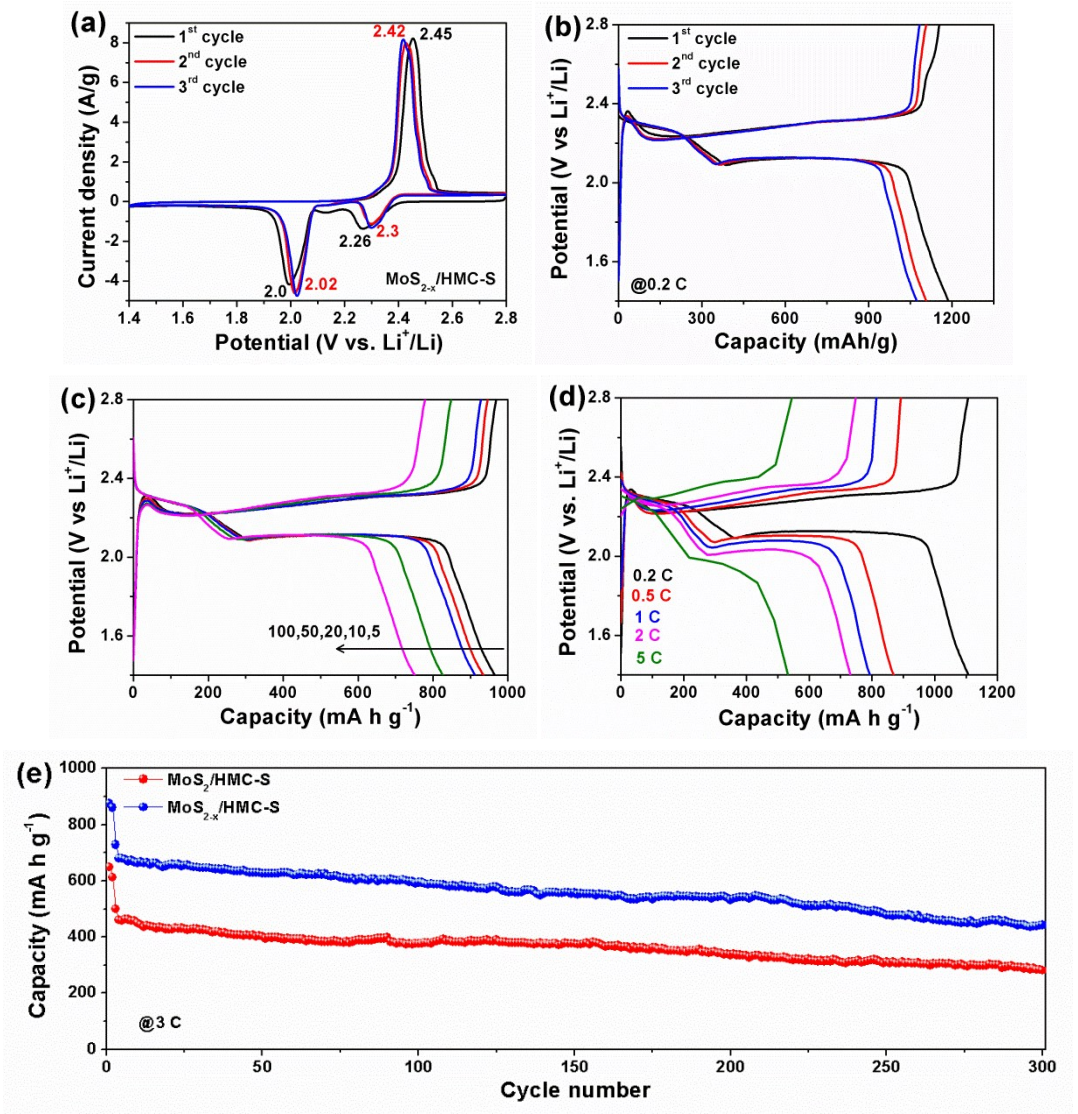

Fig. S10 CV curves of Li-S cells with (a) MoS_{2-x}/HMC-S and (b) MoS_2/HMC-S cathodes at varying scan rates. (c) Plots of peak current (i_p) with the square root of the scan rate ($\upsilon^{1/2}$) of them.

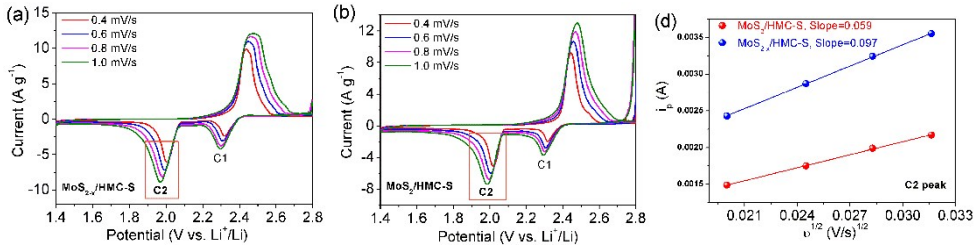

Fig. S11 EIS spectra and equivalent circuit model (inset) of the three Li-S cells with HMC-S, MoS_2/HMC-S and MoS_{2-x}/HMC-S cathodes, respectively. The hollow spheres and solid lines represent the raw and fitted data, respectively. The symbols of R_s, *CPE*, R_{ct}, and *W* in the inset represent the series resistance, constant phase element, charge transfer resistance at interface, and Warburg resistance, respectively.

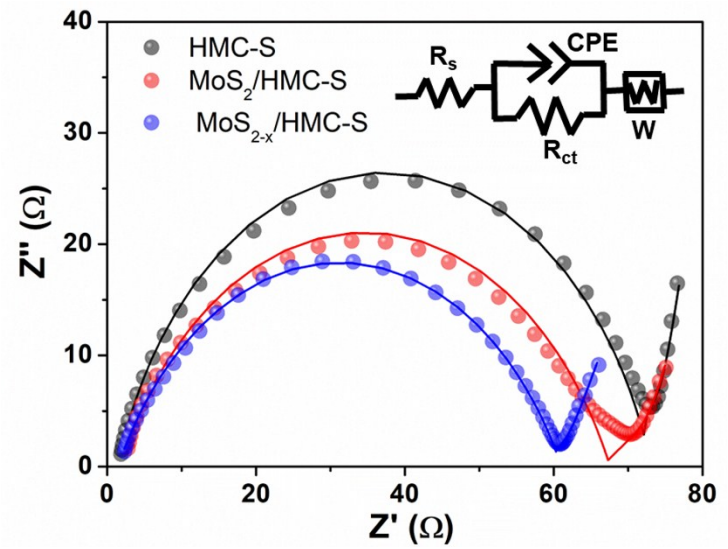

Table S1 Summary of pore characteristics of the as-prepared samples.

Sample Name	BET ($m^2 g^{-1}$)	Pore volume ($cm^3 g^{-1}$)	Average pore size (nm)
HMC	892.1	1.31	6
MoS_2/HMC	146.6	0.39	3.7/5.5
MoS_{2-x}/HMC	179.1	0.4	3.7/5.5

Table S2 Electrochemical performance comparison of our MoS_{2-x}/HMC-S cathode with recent literature.

Cathode	Capacity (mA h g^{-1}) at 0.5 C	Capacity (mA h g^{-1}) at 1 C	Capacity (mA h g^{-1}) at 2 C	Capacity (mA h g^{-1}) at 5 C	Reference
MoS_{2-x}/HMC	**876**	**800**	**730**	**528.3**	**Our work**
$TiO_2/BaTiO_3$ junction	842	704	607	493	[5]
MoS_2@rGO foam	860	750	660	NP	[6]
rGO/SnS_2/TiO_2 hybrid	697.5	562.8	449.3	306.3	[7]
C/MoS_2/CNTs hybrid	906	801.8	671.6	NP	[8]
rGO/VS_2 composite	1133	987	875	401	[9]
MXene/1T-2H MoS_2-C	1014.1	905.1	677.2	NP	[10]
$BaSr_{0.5}Co_{0.8}Fe_{0.2}O_{3-\delta}$	853	796	753	351 (4C)	[11]
PEDOT/MnO_2 hybrid	1002	896	767	631 (3C)	[12]

NP: Not Provided.

References

1. H. Zhang, O. Noonan, X. Huang, Y. Yang, C. Xu, L. Zhou and C. Yu, *ACS Nano*, 2016, **10**, 4579-4586.
2. H. B. Lin, L. Q. Yang, X. Jiang, G. C. Li, T. R. Zhang, Q. F. Yao, G. W. Zheng and J. Y. Lee, *Energy Environ. Sci.*, 2017, **10**, 1476-1486.
3. M. D. Segall, P. J. D. Lindan, M. J. Probert, C. J. Pickard, P. J. Hasnip, S. J. Clark and M. C. Payne, *J. Phys. Cond. Matt.*, 2002, **14**, 2717-2744.
4. S. J. Clark, M. D. Segall, C. J. Pickard, P. J. Hasnip, M. J. Probert, K. Refson and M. C. Payne, *Zeitschrift Fur Kristallographie*, 2005, **220**, 567-570.
5. H.-E. Wang, K. Yin, X. Zhao, N. Qin, Y. Li, Z. Deng, L. Zheng, B.-L. Su and Z.-G. Lu, *Chem. Commun.*, 2018, **54**, 12250-12253.
6. Y. You, Y. Ye, M. Wei, W. Sun, Q. Tang, J. Zhang, X. Chen, H. Li and J. Xu, *Chem. Eng. J.*, 2019, **355**, 671-678.
7. P. Wu, L. H. Chen, S. S. Xiao, S. Yu, Z. Wang, Y. Li and B. L. Su, *Nanoscale*, 2018, **10**, 11861-11868.
8. J. Ren, Y. Zhou, L. Xia, Q. Zheng, J. Liao, E. Long, F. Xie, C. Xu and D. Lin, *J. Mater. Chem. A*, 2018, **6**, 13835-13847.
9. Z. Cheng, Z. Xiao, H. Pan, S. Wang and R. Wang, *Adv. Energy Mater.*, 2018, **8**,

1702337.
10. Y. Zhang, Z. Mu, C. Yang, Z. Xu, S. Zhang, X. Zhang, Y. Li, J. Lai, Z. Sun, Y. Yang, Y. Chao, C. Li, X. Ge, W. Yang and S. Guo, *Adv. Funct. Mater.*, 2018, **28**, 1707578.
11. L. Kong, X. Chen, B.-Q. Li, H.-J. Peng, J.-Q. Huang, J. Xie and Q. Zhang, *Adv. Mater.*, 2018, **30**, 1705219.
12. M. Yan, Y. Zhang, Y. Li, Y. Huo, Y. Yu, C. Wang, J. Jin, L. Chen, T. Hasan, B. Wang and B.-L. Su, *J. Mater. Chem. A*, 2016, **4**, 9403-9412.